

Breathing sediments: The control of diffusive transport across the sediment–water interface by periodic boundary-layer turbulence

Andreas Lorke,¹ Beat Müller, Martin Maerki, and Alfred Wüest

Limnological Research Center, EAWAG, Kastanienbaum, Switzerland

Abstract

We performed combined in situ measurements of bottom boundary-layer turbulence and of diffusive oxygen fluxes at the sediment–water interface in a medium-sized mesotrophic lake. The turbulence was driven by internal seiching with a period of 18 h. This periodic forcing, a prominent feature of enclosed water bodies, led to distinct deviations of the structure and the dynamics of the bottom boundary layer from the classical law-of-the-wall theory. A major feature was a phase lag between the current velocity and the turbulent energy dissipation of approximately 10% of the seiching period (1.5–2 h). The oxygen flux into the sediment was controlled by the diffusive boundary layer, the thickness of which varied between 0.16 and 0.84 mm during the course of a seiching period, and was strongly affected by the periodic bottom boundary-layer turbulence. The rate of dissipation of turbulent energy in the bottom boundary layer allowed us to define the Batchelor length for dissolved oxygen, which quantifies the smallest scales of oxygen fluctuations and provides an appropriate scaling for the diffusive boundary-layer thickness and the corresponding oxygen fluxes. An analysis of the governing time scales revealed the importance of turbulence in controlling the small-scale spatial heterogeneity of the diffusive fluxes. Higher turbulence causes the diffusive boundary layer (DBL) to follow the sediment topography more smoothly, resulting in an increased area-averaged flux due to the greater effective surface area.

After surface zones, the bottom boundary layer (BBL) is the second prime site for animals, plants, and microorganisms in natural waters. From a physical and geochemical point of view, the importance of the BBL is twofold. First, the BBL is a major energy sink for basin-scale currents due to bottom friction and also due to the breaking of propagating internal waves on sloping bottoms (Imberger 1998). Consequently, the level of turbulence is enhanced in the BBL compared with the interior water body. Second, the BBL controls the exchange of solutes and particles between water and sediment. The sediment surface is usually an enormous sink of oxygen due to the processes caused by the decomposition of organic matter. Furthermore, the redissolution and subsequent vertical transport of ions and other solutes supply primary producers with nutrients and affect the stability of the water column by chemical (salinity) stratification (Wüest and Gloor 1998).

Especially in eutrophic and mesotrophic systems with

high turnover rates of organic matter, the associated high sediment–water fluxes can become transport limited (Wüest and Lorke 2003). The vertical transport within the turbulent BBL is dominated by eddy diffusion, which depends on the dissipation rate of turbulent kinetic energy and the stability of the density stratification. Close to the sediment, however, turbulent eddy diffusivity decreases due to laminarization of the flow at small scales. Approaching the sediment, the vertical transport becomes dominated by molecular diffusion, which depends mainly on the type of solute and the temperature. A diffusive boundary layer (DBL) with a height δ_{DBL} of up to a few millimeters develops, which can limit the total vertical flux and become the bottleneck of sediment–water fluxes.

Assuming a constant molecular diffusivity D , the vertical flux J of a particular solute (such as oxygen) through the DBL can be expressed by

$$J = D(C_{\infty} - C_0)/\delta_{\text{DBL}} \quad (1)$$

with C_{∞} and C_0 being the concentrations in the bulk fluid (BBL) and at the immediate sediment–water interface, respectively (Boudreau and Jørgensen 2001). Assuming no additional consumption or production within the DBL, the vertical concentration gradient $\partial C/\partial z$ should be constant and the concentration should decrease linearly toward the sediment surface (Steinberger and Hondzo 1999). The ratio $\beta = D/$

¹ Corresponding author (andreas.lorke@eawag.ch).

Acknowledgments

We thank C. Dinkel and M. Schurter for their great help in the field. D. McGinnis kindly improved the English. We gratefully acknowledge the helpful criticism of two unknown reviewers. The work was financially supported by the Swiss National Science Foundation 2000-067091.01 and by EAWAG.

δ_{DBL} , i.e., the factor of proportionality between the flux and the concentration difference ($C_{\infty} - C_0$), is defined as the mass transfer coefficient. Because the solute concentrations within the BBL vary slowly in most water bodies, mainly the DBL thickness determines the sediment–water flux.

The DBL was studied by using oxygen microelectrodes under controlled conditions in the laboratory (Jørgensen and Revsbech 1985; Sweerts et al. 1989; Jørgensen and Des Marais 1990; Steinberger and Hondzo 1999; Røy et al. 2002) as well as under natural conditions in the field (Reimers et al. 1986; Archer et al. 1989; Gundersen and Jørgensen 1990; Archer and Devol 1992). Although almost all of these investigations emphasized the importance of hydrodynamics for the thickness and structure of the DBL, there are no combined field experiments of BBL turbulence and DBL dynamics. The laboratory measurements of Sweerts et al. (1989), Gundersen and Jørgensen (1990), Hondzo (1998), as well as Steinberger and Hondzo (1999), however, revealed a significant decrease of δ_{DBL} for increasing flow velocities. The latter two studies found a linear dependence between the mass transfer coefficient β and the turbulent friction velocity u_{*} based on comprehensive measurements in a laboratory flume.

As pointed out, turbulent mixing within the BBL controls the upper limit of the DBL and therefore its thickness. On the other hand, the boundary-layer turbulence is forced by large-scale currents, which are very often periodic. Such currents are predominantly produced by basin-scale internal waves (internal seiches) in enclosed water bodies (MacIntyre et al. 1999; Gloor et al. 2000; Lorke et al. 2002) or by tides or inertial currents in estuaries and coastal oceans (Peters 1999; Simpson et al. 2000). Consequently, it can be expected that the periodicity of basin-scale currents and the resulting periodic BBL turbulence undulates the sediment–water fluxes by affecting the thickness of the DBL within the lowest millimeter above the sediment (Higashino et al. 2003). This cascading process has a high impact on measurement strategies for the assessment of the sediment oxygen demand as well as on lake and reservoir management and restoration tasks. Proper parameterization of the sediment–water flux as a function of BBL dynamics is also required for water-quality modeling.

This article presents the first in situ investigation of BBL flow and turbulence combined with simultaneous oxygen microelectrode measurements of the DBL. The measurements were conducted in a medium-sized mesotrophic lake and cover more than one complete cycle of internal seiching with a period of about 18 h. The periodically varying turbulence and especially its impact on the sediment–water oxygen exchange is analyzed and discussed in this article.

Study site and instrumentation

The measurements were carried out for 25 h on 13 August 2002–14 August 2002 in Lake Alpnach, a medium-sized subbasin of Lake Lucerne in central Switzerland. It has an elliptical shape with axes lengths of 5 and 1.5 km and a maximum depth of 34 m.

Lake Alpnach is mesotrophic and hence has a high turn-

over rate of organic carbon, resulting in high sediment oxygen demand and a potentially short oxygen penetration depth into the sediment of less than a few millimeters. This top sediment layer is typically characterized by porosities >0.95 . In addition to its geochemistry, the strongly pronounced seiching (Münnich et al. 1992; Gloor et al. 1994) resulting from a daily wind forcing along the main axis makes Lake Alpnach an ideal site for the present study.

The experimental setup, described in more detail below, consisted of the combined and simultaneous observations of the BBL currents, the turbulence level, and the molecular sediment–water exchange fluxes. These measurements were realized by deploying two Acoustic Doppler Current Profilers (ADCPs) and a benthic lander, capable of measuring oxygen microstructure profiles across the sediment–water interface, as well as by casting temperature microstructure and regular CTD (conductivity–temperature–depth) profiles. All instruments were operated within a radius of about 100 m at a site close to the center of the lake at a local depth of 32.2 m.

ADCP measurements—A 600-kHz RDI Workhorse ADCP was deployed directly onto the sediment facing upward. The high-resolution pulse-coherent mode (RDI mode 5) with a bin size of 0.1 m was used, enabling a measurement range of 0.6–8.1 m above the sediment (31.6–23.7 m depth). Groups of three pings were averaged internally, and the averaged data were recorded every 2 s. In addition, a 1.5-MHz Nortek NDP was mounted on a tripod facing downward, resolving a range between 0.05–2.2 m above the sediment (32.15–30 m depth) with a vertical bin size of 0.04 m. The NDP was also operated in high-resolution pulse-coherent mode (Lorke et al. 2002) with a profile interval of 9 s, averaged over six pings.

Temperature microstructure and CTD measurements—Temperature microstructure profiles were measured with a pair of fast response thermistors (FP07, Thermometrics) on an adapted SEABIRD SBE-9 CTD profiler (Kocsis et al. 1999). The probe was operated freely, sinking with a speed of 8 cm s^{-1} from a 20-m depth to about 0.15 m above the sediment. The sampling frequency was 96 Hz, and profiles were collected every 15 min.

A SEABIRD SBE-19 CTD was used to measure profiles of temperature, conductivity, oxygen concentration, pH, and light transmission throughout the entire water column about every 2 h.

Oxygen microstructure at the lake bottom—A benthic lander system equipped with two Clark-type oxygen probes (OX25, Unisense S/A, Denmark) spaced 25 mm apart, was employed to measure oxygen profiles across the sediment–water interface with submillimeter resolution (Müller et al. 2002). To avoid disturbances of one sensor by the other, the lander was oriented in such a manner that the plane formed by the sensor pair was perpendicular to the direction of the main bottom current velocity along the main axis of the lake.

Oxygen profiles were measured with a spatial resolution of $60 \mu\text{m}$. Two hundred sixty single readings were recorded with a frequency of 6.3 Hz at each depth, immediately after

the sensors reached the preset stepping position. The time required for the completion of an entire profile was 70–90 min. The stepping motor and the electrode signals were monitored on-line from the ship by computer, allowing ad hoc vertical positioning of the sensors for the individual profiles. The starting point of a profile was set a few millimeters above the sediment, and the profile was completed when constant low electrode signals were reached within the sediment. The two sensors were deliberately staggered by a tiny vertical offset with respect to the sediment surface.

Seventeen oxygen microprofiles, each consisting of 90–110 depth bins, were recorded between 13 August 2002, 1300 h, and 14 August, 1400 h. A sediment core (5.8 cm in diameter) was taken every 3 h using a gravity corer (Uwitech) to determine the oxygen concentration in the water directly overlying the sediment by Winkler titration.

Data processing

Dissipation rate ε —Dissipation rates of turbulent kinetic energy ε were calculated from the temperature microstructure profiles using the Batchelor method and from the two ADCPs using the inertial dissipation method. Both methods have been described in different research articles in great detail and are therefore only briefly summarized.

The Batchelor method is based on the existence of a universal form of the temperature fluctuation spectrum near the high frequency (diffusive) cut-off, which depends mainly on ε (Batchelor 1959). The measured temperature microstructure profiles were segmented using fixed and overlapping segmentation lengths of 512 data points, corresponding to ≈ 45 -cm-long profile sections. The respective fluctuation spectra in the wave-number domain were fitted to the theoretical Batchelor spectrum with ε and χ (the dissipation rate of temperature variance) as the fitting parameters. The probe, the data acquisition, and the data processing procedure were described in detail in Kocsis et al. (1999) and Jonas et al. (2003).

Similarly, the inertial dissipation method is based on the universal form of the velocity spectrum within the inertial subrange (Kolmogorov spectrum), which depends solely on ε (Tennekes and Lumley 1973). Segments of the measured time series of the two-dimensional horizontal current velocities at different depths were first analyzed for the main current direction, and subsequently the velocity vectors were projected relative to the along and transversal directions. The dissipation rate ε was estimated by fitting the respective wave-number spectra of current velocity fluctuations in the inertial subrange to the Kolmogorov spectrum (Wolk et al. 2002; Jonas et al. in press).

DBL thickness and the flux of oxygen into the sediment—The flux of oxygen, the thickness of the DBL, and the penetration depth of oxygen into the sediment were determined from the microelectrode profiles. The absolute oxygen concentrations were estimated by calibrating the bottom water (bulk) concentration from the uppermost part of the microprofiles with those values determined by Winkler titration of the sediment core water samples.

The observed profiles were fitted to a steady-state one-

dimensional diffusion and zero-order reaction model adapted from Epping and Helder (1997). A depth-independent consumption rate of oxygen in the sediment was used as the fitting parameter. Within the sediment, a constant consumption rate leads to a quadratic decrease of oxygen as a function of depth. The flux of oxygen into the sediment, which is necessary to sustain this consumption rate, was assumed to be equal to the diffusive flux across the DBL. Hence, the effective DBL thickness could be calculated by

$$\delta_{\text{DBL}} = \frac{D(C_{\infty} - C_0)}{\sqrt{2C_0D_sR}} \quad (2)$$

with R [$\text{g m}^{-3} \text{s}^{-1}$] denoting the constant oxygen consumption rate within the sediment and D_s being the reduced molecular diffusivity in the pore water ($D_s = D/(\phi F)$), where ϕ [–] and F [–] represent sediment porosity and resistivity formation factor (tortuosity), respectively. The combined effect of porosity and tortuosity on the diffusion of ions was estimated to be only 5% for the top few millimeters of the sediment (Maerki et al. in press).

R was estimated by fitting a second-order polynomial to the pore-water oxygen profile between the sediment surface and the maximum oxygen penetration depth. Standard deviations of the 260 measurements at each depth were helpful qualitative indicators to define the sediment–water interface. The concentration variance decreased drastically due to the diminishing eddy diffusion when the sensor approached the sediment surface and remained at a minimum in the pore water (Gundersen and Jørgensen 1990; Müller et al. 2002). Two such processed representative sample profiles are shown in Fig. 1.

Observations

BBL dynamics—The time series of the horizontal current components are shown in Fig. 2. The currents were dominated by along-lake seiching with a period of approximately 18 h. At the end of the observation, a moderate wind, starting around 1030 h on 14 August 2002, slightly disturbed the regularity of the seiching. The 18-h period is probably the intrinsic period of the first horizontal/second vertical mode internal seiche, as observed in Lake Alpnach by Münnich et al. (1992). The maximum current speed at 1 m above the sediment was 30 mm s^{-1} . Both current components in Fig. 2 clearly show higher levels of variance during periods of higher velocities, most probably associated with enhanced levels of turbulence.

Two profiles of the dissipation rates ε based on temperature microstructure and current velocity fluctuations are plotted in Fig. 3 together with the current velocities for high and low levels of turbulence, respectively. The two microstructure-based dissipation profiles are almost identical within the stratified hypolimnion. Within the turbulent BBL, which is restricted up to a range of 2 m above the sediment, the dissipation rate changes by more than two orders of magnitude during the course of the seiching. The difference between the microstructure- and ADCP-based dissipation estimates can be attributed to the two different measurement and averaging techniques for sampling intermittent turbulence.

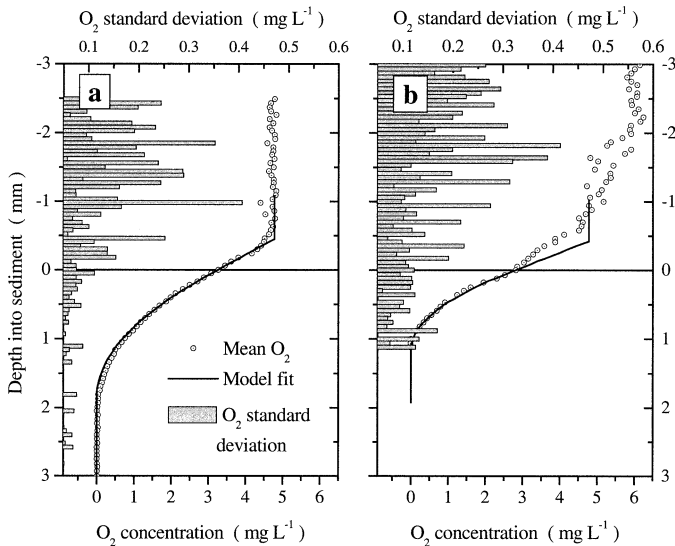


Fig. 1. Two O_2 microprofiles (circles) recorded at 32-m depth in Lake Alpnach simultaneously with two sensors (3rd profile, 13 August 1530–1700 h). Horizontally, the sensors were positioned 25 mm apart, and the difference in the vertical positions corresponded to a time difference of about 10 min. The lines are model results. The bars represent standard deviations calculated from the 260 values measured at each depth. Measurements in profile (b) show an irregular profile in the water overlying the sediment (*see* Discussion). The DBL thicknesses calculated from these profiles were (a) 0.45 mm and (b) 0.42 mm.

Whereas the temperature microstructure method measures instantaneous values of ε , averaged over a depth interval (segment length ≈ 45 cm) and is most sensitive to the high-wave number range of the respective fluctuation spectrum, the inertial dissipation method is averaging over the applied time series intervals (≈ 19 min) and is most sensitive to the lowest respective wave number range. The naturally occurring intermittency of the turbulence can only be resolved by the microstructure method, whereas the inertial dissipation-based estimate is determined mainly by the maximum dissipation within the respective time interval. The two microstructure-based dissipation profiles in Fig. 3a are hourly averages (average of four subsequent microstructure profiles). The individual estimates (not shown) follow smoothly the ADCP-based dissipation profiles as an upper bound of their intermittent fluctuations.

The particular form of the profiles can deviate substantially from the classical law-of-the-wall scaling ($\varepsilon \sim z^{-1}$; Imboden and Wüest 1995) and the observed current velocity profiles in Fig. 3b show distinct current speed maxima as typical features of an oscillatory boundary layer (Lorke et al. 2002; Mellor 2002). In Stoke's solution for an oscillatory boundary layer (Schlichting 1962), these maxima continue in an oscillatory structure with decreasing amplitude for increasing heights above the sediment. This structure is, at least partially, resolved in the current speed profile measured at 0930 h in Fig. 3b. Thus, the logarithmic boundary layer seems restricted to the lowest 0.5 m above the sediment. The minimum in the dissipation profile measured at 0930 h in Fig. 3a between 29 m and 30 m depth can be related to the

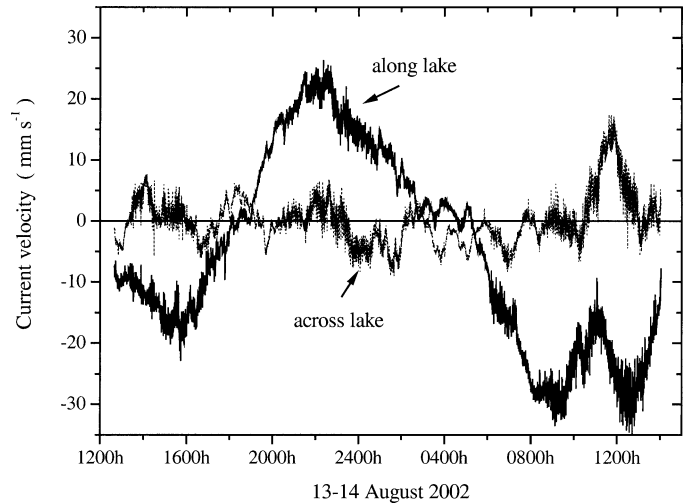


Fig. 2. Horizontal current velocities measured at 1-m height above the sediment by the NORTEK ADCP. The velocities, originally measured in earth coordinates, were transformed into the along-lake and across-lake components by local rotation.

reduced vertical current shear expected to occur at the depth of the current speed maximum.

The time series of current speed and direction measured by both ADCPs agreed well (not shown), whereas the vertical structure of the measured current profiles deviated sometimes significantly within the overlapping range of the measurements (Fig. 3b). Those differences, however, are within the range of the temporal (and spatial) dynamics of the currents, as indicated by the overlapping standard deviations in Fig. 3b, and may be attributed to the distance between the two instrument deployments.

The deviations from steady-state BBL turbulence (law-of-

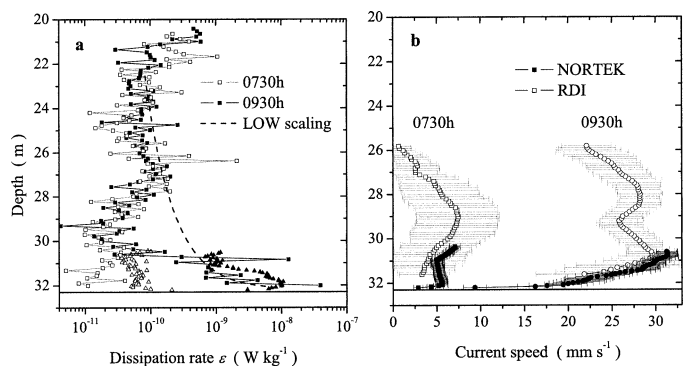


Fig. 3. (a) Two sample profiles of turbulent kinetic energy dissipation ε as estimated from the temperature microstructure measurements (squares) and from the NORTEK ADCP (triangles). The two microstructure-based dissipation profiles show hourly averages around the times given in the legend and were chosen to represent a high and low energetic state of the BBL. The law-of-the-wall scaling ($\varepsilon \sim 1/z$) is added to the high-energetic profile. (b) The corresponding profiles of the current speed, averaged over 15 min, as estimated by the NORTEK and RDI ADCPs. The error bars show the respective standard deviations. The smaller deviations of the NORTEK data result from the higher degree of internal averaging in the instrument prior to recording.

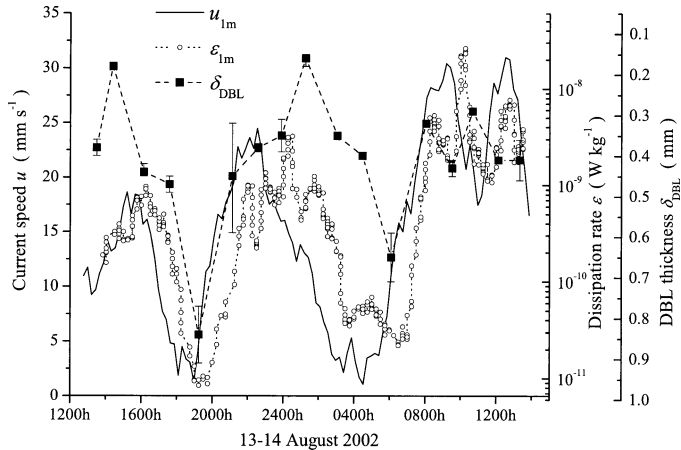


Fig. 4. Time series of the current speed u , the dissipation rate ε , and the thickness of the DBL δ_{DBL} (mean values and variance range of the respective two individual estimates) for the entire measurement period. u and ε were measured at a height of 1 m above the sediment. Note the logarithmic axis scale for the dissipation rate and the reversed axis for the DBL thickness.

the-wall scaling) can be attributed to the effect of the seiche-induced, slowly oscillating forcing, which was analyzed and discussed in greater detail by Lorke et al. (2002). Basically, they showed that the BBL of such a low-energetic and periodically forced system is not in steady-state, though the forcing periods are relatively long. As a consequence, the form and scaling of the velocity profiles at some distance to the sediment deviate significantly from the logarithmic form. The local and temporal imbalance of production and dissipation of turbulent kinetic energy leads to a phase lag between the forcing (seiche-induced currents) and the turbulent energy dissipation. This phase lag of 1–2 h is well resolved in the measurements (Fig. 4 and discussion below) and confirms the former observations and model simulations of Lorke et al. (2002).

DBL fluxes—As depicted in Fig. 1b, the DBL thickness δ_{DBL} was not well defined in some profiles, particularly not during periods of weak turbulence. Because of the occasional occurrence of irregularly formed profiles, it was in many cases not possible to directly estimate the DBL thickness by fitting a constant gradient to an appropriate section of the oxygen profile (Fig. 1b). Hence, the diffusion and reaction model, as described in the data processing section, was used to estimate δ_{DBL} for the subsequent analysis and discussion.

The estimates of δ_{DBL} according to Eq. 2 varied between 0.16 mm and 0.84 mm during the entire period of measurements. However, the total oxygen flux into the sediment, as estimated by Eq. 1, varied between only 6 and 13.2 mmol $\text{m}^{-2} \text{d}^{-1}$ and did not follow the same temporal dynamics as δ_{DBL} , since the oxygen concentration in the BBL (C_{∞}) changed due to seiche-induced oxygen-isoline displacements. This additional effect of seicheing on the sediment–water oxygen flux is a function of the particular measurement site and the hypolimnetic oxygen stratification and will not be discussed here. The overall mean of the oxygen flux

was 8.9 mmol $\text{m}^{-2} \text{d}^{-1}$. The average oxygen penetration depth into the sediment was 1.67 mm.

The main contributions to the uncertainty of δ_{DBL} can be estimated from Eq. 2. As determined by independent measurements in the laboratory (Maerki et al. in press), the effect of porosity and tortuosity on the pore-water diffusivity is only 5% and hence the uncertainties in D_s and D can be neglected. Similarly, the fit of the zero-order reaction model to the pore-water oxygen profiles resulted in very robust estimates of R with least-square fitting errors of only a few percent and small differences between the respective quasi-simultaneously measured profiles. The errors, however, were introduced by the estimated oxygen concentrations C_0 and C_{∞} . C_0 is determined by the choice of the location of the sediment–water interface and a vertical offset of ± 0.2 mm typically results in an error of about 10% in δ_{DBL} . The main uncertainty in δ_{DBL} , however, is introduced by the estimate of the hypolimnetic oxygen concentration C_{∞} . As illustrated in Fig. 1, the oxygen profiles above the sediment are subject to strong temporal variations due to horizontal advection and the assumed boundary condition of a constant hypolimnetic oxygen concentration C_{∞} was not valid throughout the time required to finish one profile. However, for an estimate of an effective thickness of the DBL according to Eq. 2, a proper estimate of an average concentration C_{∞} is essential. An error of 10% in C_{∞} will typically result in a 30% error of δ_{DBL} . This uncertainty is not produced by the accuracy of the measurements (the influence of the drift of the oxygen electrodes between the calibrations can be neglected), but by the conceptual problem of nonstationary conditions. However, it should be noted that the basic assumption for the entire procedure of calculating δ_{DBL} on the basis of the pore-water diffusion–reaction model according to Eq. 2 is stationarity, i.e., $\partial C/\partial t = 0$ at all depths.

Discussion

Figure 4 shows the time series of the near-sediment dissipation rate and the current velocity together with the estimated DBL thickness. This figure not only reveals a clear correlation but also a pronounced phase lag between all three quantities. Corresponding to the measurements and simulations of Lorke et al. (2002), the phase lag is most obvious between the current and dissipation, where the turbulent dissipation rate lagged between 1 and 2 h behind the current.

A similar but less pronounced phase lag relative to the current speed also occurs for the DBL thickness, especially during periods of decreasing current velocities. There, δ_{DBL} more likely follows the delayed decrease of turbulent dissipation rather than the current velocity. The estimation of the effective DBL thickness, using the sediment oxygen consumption model, introduces a certain delay (and subsequently a phase shift) between the actual forcing and δ_{DBL} due to the diffusive pathway of the oxygen through the sediment. This delay, however, is less than approximately 15 min and cannot account for the observed phase shift of more than 1 h as indicated in Fig. 4. In order to account for this artificially introduced delay at least partially, the time of measurement for δ_{DBL} was set to the time when the electrode contacted the sediment surface.

The scaling of δ_{DBL} —Nearly all of the previous studies relating the DBL thickness δ_{DBL} or the resulting mass transfer coefficient $\beta = D/\delta_{DBL}$ to the flow conditions near the sediment–water interface have been conducted in the laboratory (Jørgensen and Revsbech 1985; Jørgensen and Des Marais 1990; Hondzo 1998; Mackenthun and Stefan 1998; Steinberger and Hondzo 1999; Røy et al. 2002). Sediment samples were exposed to defined flow conditions in laboratory flumes, and the measured diffusive oxygen flux was related to the flow velocity or to the turbulent friction velocity u_* of a law-of-the-wall layer. Depending on the roughness of the sediment surface, both parameters are related, assuming that the BBL is in steady state with the forcing.

This assumption is justified for streams and might also be a good approximation for high-energetic systems, such as estuaries and tidal channels. However, in less energetic and periodically forced aquatic systems, such as lakes and reservoirs, it is not the current velocity but the BBL turbulence that forces the DBL thickness (Fig. 4). Lorke et al. (2002) showed that estimating u_* from measured velocity profiles using the profile method is not appropriate for quantifying turbulence in those systems and under those conditions. Hence, the application of the proposed DBL scaling, which can be summarized in the form $\beta \sim u_* Sc^a$ (Boudreau 2001) with $Sc = \nu/D$ denoting the Schmidt number, is not useful in this context.

An alternative scaling was proposed by Hearn and Robson (2000), who used the Batchelor length for oxygen L_B

$$L_B = 2\pi \left(\frac{\nu D^2}{\varepsilon} \right)^{1/4} \quad (3)$$

(ν is the kinematic viscosity and D the molecular diffusivity of oxygen; both are temperature dependent) to scale δ_{DBL} in a numerical model. L_B describes the smallest length scales of turbulent tracer (concentration) fluctuations before molecular diffusion smoothes the remaining gradients. If the level of turbulence, expressed by the dissipation rate ε is enhanced, concentration fluctuations can persist at smaller scales. Well-resolved spectra of temperature fluctuations reveal a clear cut-off at wave numbers that correspond to the Batchelor length for temperature. This cut-off, where the spectral energy decays strongly ($\sim \exp(-k^2)$) for increasing wave numbers k , can actually be used to determine the dissipation rate ε (De Szoeke 1998). Based on the same arguments, L_B can be used to scale δ_{DBL} , however with the conceptual limitation that L_B was defined for open flow and not at a rigid boundary.

Because we were not able to resolve ε close enough to the sediment with direct measurements, we used the ADCP-based dissipation rate estimates at 0.5 m above the bottom and law-of-the-wall scaling ($\varepsilon \sim z^{-1}$) to extrapolate ε down to the viscous sublayer at a height δ_ν with

$$\delta_\nu = 11 \nu / u_* \quad (4)$$

(Chriss and Caldwell 1984), at about 1 cm above the sediment. The applicability of the law-of-the-wall scaling within the lowest 0.5 m above the sediment was confirmed with numerical simulations by Lorke et al. (2002), who showed

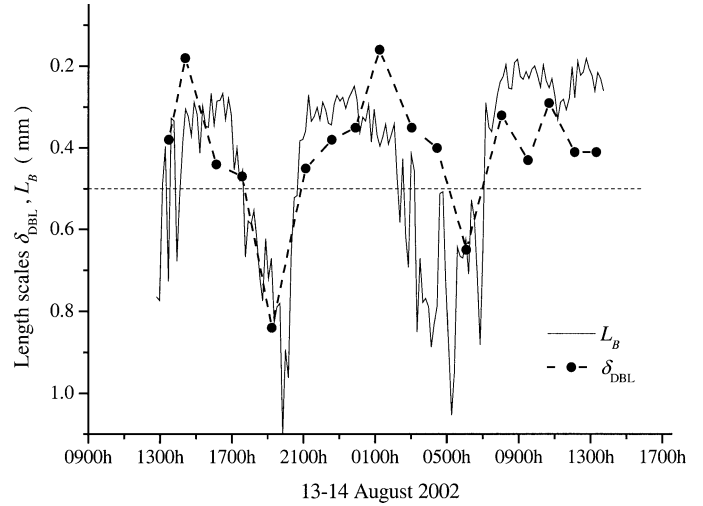


Fig. 5. Time series of the estimated DBL thicknesses δ_{DBL} and the Batchelor length scale L_B . L_B was estimated according to Eq. 3 using dissipation rates ε extrapolated from a measurement height of 0.5 m above the sediment to a height of 1 cm assuming law-of-the-wall scaling. The height of 1 cm corresponds to the average height of the viscous sublayer within which ε can be assumed to be constant. The dashed line represents the low-energy limit, where no law-of-the-wall characteristics could be observed in individual dissipation profiles, indicating that the respective values of L_B below that line (L_B greater than the average low-energy threshold) might be underestimated by the applied extrapolation.

that the modifications of the current velocity and dissipation rate profiles due to the oscillatory structure of the flow start at a certain height above the sediment, which was estimated to be about 0.5 m in the same lake and under comparable conditions. Below that height, the steady-state law-of-the-wall scaling applies to both the current velocity and dissipation rate profiles. Figure 3 illustrates that the law-of-the-wall extrapolation is well justified during the high-energetic periods; however, during the low-energetic periods, individual dissipation profiles do not necessarily show any law-of-the-wall characteristics. The deviations are either due to laminarization of the flow or due to a restriction of the turbulent BBL to unresolved regions of the flow close to the sediment. For those profiles, we assume that the law-of-the-wall extrapolation can be applied on average, taking a possible underestimation of L_B into account.

The Batchelor length, based on the extrapolated dissipation rate at 1 cm above the bottom, is plotted together with the estimated DBL thicknesses in Fig. 5. By considering all the uncertainties and especially the spatial gap of about three orders of magnitude between the points of measurements of dissipation and oxygen (1 m vs. $O(1)$ mm above the sediment, respectively), the agreement between both length scales is encouraging. Both scales cover the same dynamic range and exhibit the same temporal dynamics, enabling the Batchelor length scale to be used at least as a first-order approximation of the thickness of the DBL.

The proposed scaling of $\delta_{DBL} = L_B$ also leads to the conclusion that the thickness of the viscous sublayer δ_ν scales with the Kolmogorov length $L_K = 2\pi(\nu^3/\varepsilon)^{1/4}$. Actually, by evaluating the law-of-the-wall $\varepsilon = u_*^3/\kappa z$ ($\kappa \approx 0.41$, von

Karman constant; Imboden and Wüest 1995) at a height $z = \delta_\nu$ and using it to replace u_* in Eq. 4 results in $\delta_\nu \approx 7.5(\nu^3/\varepsilon)^{1/4}$, which is equal to L_K as defined above within the errors given by Chriss and Caldwell (1984).

As a consequence of both scaling relations, it follows that the ratio $\delta_{\text{DBL}}/\delta_\nu$ is proportional to $Sc^{-0.5}$ and that δ_{DBL} can be expressed as

$$\delta_{\text{DBL}} \propto \frac{\nu}{u_*} Sc^{-1/2} \quad (5)$$

Steinberger and Hondzo (1999) obtained a similar expression, however, with an exponent of $-1/3$ instead of $-1/2$ for Sc , based on scaling arguments and the assumption that advective transport balances diffusive transport at the top of the DBL (Dade 1993). Hondzo (1998) applied a conceptual model of the mass transfer near the sediment–water interface by streamwise vortices and obtained an identical scaling relation as Eq. 5. Because Sc was almost constant in all experiments (all authors were measuring oxygen transport in water) and the main variance was produced by varying u_* , a direct proof of the dependence of δ_{DBL} on Sc is beyond the accuracy of the measurements.

Vertical diffusion versus horizontal advection—As previously pointed out and exemplified in Fig. 1b, the oxygen profiles were predominantly poorly conditioned during the periods of low turbulence. The increasing variance of the measured oxygen concentrations above the sediment surface with decreasing turbulence was confirmed by independent measurements in other lakes and was also observed by other authors. The time series shown in Gundersen and Jørgensen (1990) (their figs. 2b–2d) showed especially huge variances (temporal fluctuations) that increased with distance from the sediment surface during low-flow conditions, but almost constant oxygen concentrations at the different heights during high-flow conditions. In the same article, the authors also revealed the complex topography of the sediment surface on submillimeter scales.

The observed features in the oxygen profiles can be related to the small-scale sediment topography by considering two different processes: (i) diffusion and turbulent mixing in the vertical and (ii) advection in the horizontal. Both processes are important for the interpretation of oxygen micro-profiles measured at one particular location. So far, only the first point has been discussed—the establishment of a local DBL in relation to turbulent mixing acting vertically from above. However, these idealized local DBLs are advected by horizontal currents over changing sediment topography and are affected by the highly intermittent turbulence.

The relative importance of these two processes for local oxygen profiles can be estimated by comparing the governing time scales. The time scale for the establishment of a local DBL can be estimated as the mean diffusion time of oxygen through the DBL t_D ,

$$t_D = \frac{\delta_{\text{DBL}}^2}{D} \quad (6)$$

This results in time scales between 10 s and 5 min for the

observed values for δ_{DBL} . Setting δ_{DBL} equal to the Batchelor length scale according to Eq. 3 leads to

$$t_D = \left(\frac{\nu}{\varepsilon}\right)^{1/2} \quad (7)$$

Thus, the time scale for molecular diffusion through the respective DBL is independent of the diffusivity and hence independent of the kind of solute and should even be valid for heat.

The time scale for horizontal transport over changing sediment topography or sediment irregularities is less well defined. The distance between neighboring roughness elements will be labeled as L , whereas the advection velocity is considered to scale with the friction velocity u_* of a steady-state BBL. Although both variables are not well defined in this particular case, they will be used to estimate the time scale for advection t_h as

$$t_h \propto \frac{L}{u_*} \quad (8)$$

The law-of-the-wall scaling relates the dissipation rate at a particular height above the sediment z to the friction velocity by

$$\varepsilon = \frac{u_*^3}{\kappa z} \quad (9)$$

By using Eq. 9 to estimate ε at the outer end of the viscous sublayer at a height $z = L_K$ according to the discussion above, t_h can be expressed as

$$t_h \propto \frac{L}{\kappa(\varepsilon\nu)^{1/4}} \quad (10)$$

The ratio of the governing time scales equates to

$$\frac{t_D}{t_h} \propto \frac{\nu^{3/4}\kappa}{\varepsilon^{1/4}L} \propto \frac{L_K}{L} \quad (11)$$

Thus, the governing variables for the ratio of the time scales are ε and L . For strong turbulence and smooth sediment surfaces (ε and L are large), the local diffusive time scale t_D is small compared with the time scale for horizontal advection t_h and the DBL will correspond to the local sediment surface and turbulence. In the other case, when turbulence is weak and/or the distance between roughness elements is short, advection will dominate and an areal-averaged DBL will be observed at a distinct position (sediment surface), which does not necessarily represent the local conditions. These two different regimes are illustrated in Fig. 6 and were nicely demonstrated in Jørgensen and Des Marais (1990). Their fig. 4 clearly shows how the upper limit of the DBL follows the larger-scale roughness elements of a microbial mat, whereas small-scale structures were smoothed out completely. Furthermore, the authors observed that the DBL limit follows the small-scale topography more closely for higher flow rates, i.e., higher BBL turbulence.

Besides the two extreme cases with $t_D \gg t_h$ and $t_D \ll t_h$, a transition range exists with $t_D \approx t_h$ and is also illustrated in Fig. 6. It can be expected that the form of the oxygen profiles measured at one particular location is highly intermittent due to the temporal fluctuations of horizontal advec-

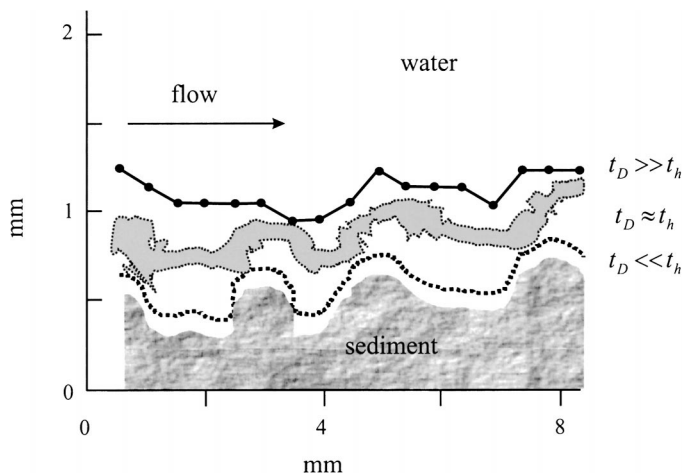


Fig. 6. Schematics of the different DBL regimes according to the relative importance of the time scales for vertical diffusion t_D and horizontal advection t_h . Note the different scaling of the vertical (relative height) and horizontal (relative distance) axes. The lines represent the upper limit of the DBL as defined by the isopleth of 90% air saturation of oxygen. The solid line with points shows data measured by Jørgensen and Des Marais (1990) and represents the advective regime. The lower dotted line, representing the diffusive regime, and the gray area, representing the transition range, are of illustrative nature only. (Parts of the figure were adopted from Jørgensen and Des Marais [1990].)

tion and vertical turbulent mixing. Exactly those sporadic horizontal intrusions, as they were observed in the data (Fig. 2b), alter the profiles and disturb the local equilibrium between molecular diffusion and turbulent mixing. Thus, it can be concluded that the varying BBL turbulence in our measurements caused a shift from the diffusion and turbulence dominated regime with $t_D \ll t_h$ to the transition range with $t_D \approx t_h$. However, a more quantitative discussion of the governing time scales would require detailed knowledge of the topography of the sediment surface in order to quantify the roughness length scale L . Additionally, it should be noted that the required time to measure one complete oxygen profile was probably much longer than the two considered time scales t_D and t_h and thus only averaged properties were resolved with our approach.

Combined in situ measurements allowed estimates of BBL turbulence and diffusive oxygen fluxes at the sediment surface in a medium-sized mesotrophic lake. The study revealed the strong relationship between the two, though they were acting on and measured at very different spatial scales. The BBL was up to 2 m thick and was forced by internal seiche with a period of 18 h. The dissipation rate of turbulent kinetic energy changed by two orders of magnitude during the course of a full seiche period. The varying level of turbulence caused the thickness of the diffusive boundary of oxygen at the sediment surface to vary by a factor of five and the local oxygen flux to vary by a factor of two.

In conclusion, these findings can be generalized. Long internal waves are a very prominent feature of all stratified and enclosed water bodies. They drive periodic currents throughout the entire water column with most of their energy dissipated in the BBL. The periodicity of the forcing causes

deviations from classical law-of-the-wall scaling relations and, in particular, results in a phase lag between the current velocity and the turbulent energy dissipation. The periodic turbulence affects the transport of solutes through the sediment–water interface in different ways. First, the actual thickness of the diffusive sublayer depends on the dissipation rate. Turbulent mixing can proceed to smaller length scales for higher levels of turbulence, and thus the DBL becomes thinner. The DBL thickness is directly (inversely) related to the mass transfer coefficient and accordingly to the total flux of solutes into or out of the sediment. Second, we have shown that turbulence also affects the relative importance of horizontal advection and vertical diffusion on small scales and therefore the degree of spatial averaging of the sediment–water fluxes. Higher turbulence causes the DBL to follow the small-scale sediment topography more smoothly, resulting in an increased area-averaged flux due to the greater effective surface area. Finally, at larger scales, the periodic dislocation of isolines by internal seiche changes the solute concentration of the water overlaying the sediment, which is the driving force for the diffusive transport.

This study has revealed some limitations of the micro-electrode technique when brought from the laboratory to the field. Although many open questions can be answered more accurately with well-defined laboratory experiments, attention must be paid to the complexity and the intermittent characteristics of natural aquatic systems. Although the problem of intermittency of naturally occurring turbulence (Baker and Gibson 1987) was omitted within this study, further measurements are needed in order to investigate its impact on measurement strategies as well as on the DBL fluxes. Most important, however, is the clear need for (i) faster oxygen profile measurements in order to resolve the high temporal and spatial dynamics of natural systems, and (ii) measurement techniques capable of resolving current velocities and diffusivities with the same spatial resolution as the oxygen microprofiles. Recent development of optical methods for oxygen concentration measurements as well as diffusivity microsensors (Boudreau and Jørgensen 2001) will facilitate promising future experiments.

References

- ARCHER, D., AND A. DEVOL. 1992. Benthic oxygen fluxes on the Washington shelf and slope: A comparison of in situ micro-electrode and chamber flux measurements. *Limnol. Oceanogr.* **37**: 614–629.
- , S. EMERSON, AND C. R. SMITH. 1989. Direct measurement of the diffusive sublayer at the deep sea floor using oxygen microelectrodes. *Nature* **340**: 623–626.
- BAKER, M. A., AND C. H. GIBSON. 1987. Sampling turbulence in the stratified ocean: Statistical consequences of strong intermittency. *J. Phys. Oceanogr.* **17**: 1817–1836.
- BATCHELOR, G. K. 1959. Small-scale variation of convected quantities like temperature in turbulent fluid. *Phil. Trans. Roy. Soc. London, A.* **5**: 113–133.
- BOUDREAU, B. P. 2001. Solute transport above the sediment–water interface, p. 104–143. *In* B. P. Boudreau and B. B. Jørgensen [eds.], *The benthic boundary layer*. Oxford University Press.

- , AND B. B. JØRGENSEN. 2001. The benthic boundary layer. Oxford University Press.
- CHRISS, T. M., AND D. R. CALDWELL. 1984. Universal similarity and the thickness of the viscous sublayer at the ocean floor. *J. Geophys. Res.* **89**: 6403–6414.
- DADE, W. B. 1993. Near-bed turbulence and hydrodynamic control of diffusional mass transfer at the sea floor. *Limnol. Oceanogr.* **38**: 52–69.
- DE SZOEKE, R. A. 1998. The dissipation of fluctuating tracer variances. *J. Phys. Oceanogr.* **28**: 2064–2074.
- EPPING, E. H. G., AND W. HELDER. 1997. Oxygen budgets calculated from in situ oxygen microprofiles for Northern Adriatic sediments. *Cont. Shelf Res.* **17**: 1737–1764.
- GLOOR, M., A. WÜEST, AND M. MÜNNICH. 1994. Benthic boundary mixing and resuspension induced by internal seiches. *Hydrobiologia* **284**: 59–68.
- , ———, AND D. M. IMBODEN. 2000. Dynamics of mixed bottom boundary layers and its implications for diapycnal transport in a stratified, natural water basin. *J. Geophys. Res.* **105**: 8629–8646.
- GUNDERSEN, J. K., AND B. B. JØRGENSEN. 1990. Microstructure of diffusive boundary layers and the oxygen uptake of the sea floor. *Nature* **345**: 604–607.
- HEARN, C. J., AND J. ROBSON. 2000. Modelling a bottom diurnal boundary layer and its control of massive alga blooms in an estuary. *Appl. Math. Mod.* **24**: 843–859.
- HIGASHINO, M., H. G. STEFAN, AND C. J. GANTZER. 2003. Periodic diffusional mass transfer near sediment/water interface: Theory. *J. Environ. Eng.* **129**: 447–455.
- HONDZO, M. 1998. Dissolved oxygen transfer at the sediment–water interface in a turbulent flow. *Water Resour. Res.* **34**: 3525–3533.
- IMBERGER, J. 1998. Flux paths in a stratified lake: A review, p. 1–18. *In* J. Imberger [eds.], *Physical processes in lakes and oceans*. American Geophysical Union.
- IMBODEN, D. M., AND A. WÜEST. 1995. Mixing mechanisms in lakes, p. 83–138. *In* A. Lerman, D. Imboden, and J. Gat [eds.], *Physics and chemistry of lakes*. Springer-Verlag.
- JONAS, T., A. WÜEST, A. STIPS, AND W. EUGSTER. 2003. Observations of a quasi shear-free lacustrine convective boundary layer: Stratification and its implications on turbulence. *J. Geophys. Res.* **108**: doi: 10.1029/2002JC001440.
- JØRGENSEN, B. B., AND D. J. DES MARAIS. 1990. The diffusive boundary layer of sediments: Oxygen microgradients over a microbial mat. *Limnol. Oceanogr.* **35**: 1343–1355.
- , AND N. P. REVSBECH. 1985. Diffusive boundary layers and the oxygen uptake of sediments and detritus. *Limnol. Oceanogr.* **30**: 111–122.
- KOCSIS, O., H. PRANDKE, A. STIPS, A. SIMON, AND A. WÜEST. 1999. Comparison of dissipation of turbulent kinetic energy determined from shear and temperature microstructure. *J. Mar. Syst.* **21**: 67–84.
- LORKE, A., L. UMLAUF, T. JONAS, AND A. WÜEST. 2002. Dynamics of turbulence in low-speed oscillating bottom-boundary layers of stratified basins. *Environ. Fluid Mechanics* **2**: 291–313.
- MACINTYRE, S., K. M. FLYNN, R. JELLISON, AND J. R. ROMERO. 1999. Boundary mixing and nutrient fluxes in Mono Lake, California. *Limnol. Oceanogr.* **44**: 512–529.
- MACKENTHUN, A. A., AND H. G. STEFAN. 1998. Effects of flow velocity on sediment oxygen demand: Experiments. *J. Environ. Eng.* **3**: 222–230.
- MAERKI, M., B. WEHRLI, CH. DINKEL, AND B. MÜLLER. In press. Influence of tortuosity on molecular diffusion in freshwater sediments of high porosity. *Geochim. Cosmochim. Acta*.
- MELLOR, G. L. 2002. Oscillatory bottom boundary layers. *J. Phys. Oceanogr.* **32**: 3075–3088.
- MÜLLER, B., M. MAERKI, C. DINKEL, R. STIERLI, AND B. WEHRLI. 2002. In situ measurements in lake sediments using ion-selective electrodes with a profiling lander system, p. 126–143. *In* M. Taillefert and T. F. Rozan [eds.], *Environmental electrochemistry*. American Geophysical Union.
- MÜNNICH, M., A. WÜEST, AND D. M. IMBODEN. 1992. Observation of the second vertical mode of the internal seiche in an alpine lake. *Limnol. Oceanogr.* **37**: 1705–1719.
- PETERS, H. 1999. Spatial and temporal variability of turbulent mixing in an estuary. *J. Mar. Res.* **57**: 805–845.
- REIMERS, C. E., K. M. FISCHER, R. MEREWETHER, K. L. SMITH, AND R. A. JAHNKE. 1986. Oxygen microprofiles measured in situ in deep ocean sediments. *Nature* **320**: 741–744.
- RØY, H., M. HÜTTEL, AND B. B. JØRGENSEN. 2002. The role of small-scale sediment topography for oxygen fluxes across the diffusive boundary layer. *Limnol. Oceanogr.* **47**: 837–847.
- SCHLICHTING, H. 1962. *Boundary layer theory*. McGraw-Hill.
- SIMPSON, J. H., T. P. RIPPETH, AND A. R. CAMPBELL. 2000. The phase lag of turbulent dissipation in tidal flow, p. 57–67. *In* T. Yanagi [eds.], *Interactions between estuaries, coastal seas and shelf seas*. Terra Scientific Publishing (TERRAPUB).
- STEINBERGER, N., AND M. HONDZO. 1999. Diffusional mass transfer at sediment–water interface. *J. Environ. Eng.* **125**: 192–200.
- SWEERTS, J.-P. R. A., V. ST LOUIS, AND T. E. CAPPENBERG. 1989. Oxygen concentration profiles and exchange in sediment cores with circulated overlying water. *Freshwater Biol.* **21**: 401–409.
- TENNEKES, H., AND J. L. LUMLEY. 1973. *A first course in turbulence*. MIT Press.
- WOLK, F., H. YAMAZAKI, L. SEURONT, AND R. G. LUECK. 2002. A new free-fall profiler for measuring biophysical microstructure. *J. Atm. Ocean. Technol.* **19**: 780–793.
- WÜEST, A., AND M. GLOOR. 1998. Bottom boundary mixing: The role of near-sediment density stratification, p. 485–502. *In* J. Imberger [eds.], *Physical processes in lakes and oceans*. American Geophysical Union.
- , AND A. LORKE. 2003. Small-scale hydrodynamics in lakes. *Ann. Rev. Fluid Mech.* **35**: 373–412.

Received: 10 December 2002

Accepted: 19 July 2003

Amended: 5 August 2003